Lookup table method of effective bandwidth for HJ-1B B08 on-board radiometric calibration

LI Jiaguo[1,2], GU Xingfa[1,2], YU Tao[1,2], HAN Qijin[3], GUO Hong[4], WANG Suying[5]

1. *Institute of Remote Sensing Applications, Chinese Academy of Science, Beijing* 100101, *China*;
2. *Graduate School of Chinese Academy of Sciences, Beijing* 100049, *China*;
3. *China Center for Resources Satellite Date & Application, Beijing* 100094, *China*;
4. *Institute of Surveying and Mapping, Henan Polytechnic University, Henan Jiaozuo* 454003, *China*;
5. *Fujian Normal University, College of Geographical Sciences, Fujian Fuzhou* 350007, *China*

Abstract: Improve HJ-1B B08 on-board absolutely radiometric calibration precision by virtue of a constructed lookup table (LUT) method that fit for HJ-1B B08 characteristic to calculate its effective bandwidth. LUT method is based on HJ-1B on-board radiometric calibration theory, pre-launched experiment datum and Planck formula. As a result, HJ-1B B08 effective bandwidths are 2.01 μm, 1.940 μm and 2.394 μm corresponding to LUT method, FWHM method and moments method (MM). LUT method has low association to blackbody temperature, and the relative difference is 0.3% between normal temperature and high temperature state. FWHM method and MM method are either higher or lower, and the calibrated top of atmospheric (TOA) radiance is either lower or higher, so they are not fit for HJ-1B B08 characteristic. LUT method gives a result that very close to field experiment, and the absolutely error is 0.04 $W \cdot m^{-2} \cdot sr^{-1} \cdot \mu m^{-1}$corresponding to approximately 0.4 K TOA radiant temperature error, so it can be better when used to HJ-1B B08 on-board absolutely radiometric calibration.

Key words: remote sensing, thermal infrared, HJ-1, calibration, effective bandwidth

CLC number: TP732 **Document code:** A

Citation format: Li J G, Gu X F, Yu T, Han Q J, Guo H and Wang S Y. 2011. Lookup table method of effective bandwidth for HJ-1B B08 on-board radiometric calibration. *Journal of Remote Sensing*, **15**(1): 60–72

1 INTRODUCTION

HJ-1 satellite constellation is designed for environmental protection and disaster prevention of China, which combines two optical satellites and one radar satellite, that "2+1" model. Numbered B (named"HJ-1B") optical satellite was launched in September 2008. HJ-1B has two optical CCD sensors and an infrared sensor IRS, which includs one thermal infrared band (B08), and the designed parameters is shown in Table 1. Accurate absolute radiometric calibration of remote sensing images is a prerequisite for quantitative applications (Lefevre et al., 2000), and all the latest generation of satellite thermal infrared sensors have on-board calibration system, such as the USA MODIS and TM optical satellite sensors, which have a full-aperture calibration system; and the Chinese FY-2 satellite, which has a semi-aperture optical calibration system (Zhang, 2006). HJ-1B used the full-aperture on-board calibration system. HJ-1B thermal infrared band measures the blackbody irradiance $N_c/(W \cdot m^{-2})$ in ground-based experiment pre-launch, while radiance $L/(W \cdot m^{-2} \cdot m^{-1} \cdot sr^{-1})$ is needed in actual quantitative remote sensing application. N_c and L conversion are needed to consider the effective bandwidth $\Delta\lambda$ of the sensor channel; and $\Delta\lambda$ accuracy directly affects the calibration accuracy. Usually $\Delta\lambda$ is calculated by normalization peak method (Peak Method), half-width method (Full Width at Half Maximum, FWHM) and Palmer (1984) proposed Moments method (MM). These methods have their own characteristics and applicability. Peak normalization method treats the maximum response as band effective wavelength, and uses the channel response of the integral area which is divided by the effective wavelength as an effective bandwidth, and large errors estimated. FWHM method treats half of the peak response ($0.5R_{max}$) as wavelength limit, and the wavelength between upper and lower bounds as effective bandwidth, and wavelength center as effective wavelength. MM method combines the features of channel response, and effective bandwidth is calculated by integral channel response with wavelength. In MM method, the effective wavelength and the wavelength boundary are clear expressed (Liang, 2009). In this paper, we study different $\Delta\lambda$ based on HJ-1B IRS B08 channel response function features by using on-board calibration data on August 5, 2009 and August 14, 2009, and analyze their suitability to improve HJ-1B IRS

Received: 2010-03-15; **Accepted**: 2010-04-21

Foundation: The China and Australia Remote Sensing Field Calibration and Validation (No. 2008DFA21540); The Chinese Defence Advance Research Program of Science and Technology,China (No. 07K00100KJ).

First author biography: LI Jiaguo (1982—), male, Ph.D. candidate. He majors in sensor calibration and LST retrieval. E-mail:jacoli@126.com

© 1994-2012 China Academic Journal Electronic Publishing House. All rights reserved. http://www.cnki.net

B08 on-board calibration accuracy.

Table 1 Designing parameters of HJ-1B B08

load	band	spectral range/μm	spatial resolution/m	swath/km	recycle/d
IRS	B08	10.5-12.5	300	720	4

2 HJ-1B ON-BOARD CALIBRATION THEORY

Function about blackbody irradiance and temperature are establishment before satellite is launched in a vacuum in the ground-based experiment, as Eq.(2) shows below. Systematic signal amplitude level of cold space is zero in theory during on-board calibration by means of observing the cold background radiation of space to determine the instrument benchmark. However, due to the shelter effect of solar panels, HJ-1B IRS can not observe the cold space, so two blackbodies are used to implement on-board calibration. One for achieving benchmarks and the other for radiance calibration. The relative position of the two blackbodies is shown in Fig.1. During on-board absolute radiometric calibration period, IRS detector collect system status P_1 (T_{c1}, DN_{c1}) at 293±5 K normal temperature of blackbody firstly and then system status at high temperature 328±5 K P_2(T_{c2}, DN_{c2}). Then P_1 and P_2 are covered to P_1'(N_{c1}, DN_{c1}) and P_2' (N_{c2}, DN_{c2}) by conversion Eq.(2) and Eq.(3), established based on ground-based test. Then substituted P_1' and P_2' into Eq.(1) to regress on-board absolute radiometric calibration coefficients: gain g and offset b. Benchmark and calibration blackbodies' emissivities ε_c are greater than 0.95, and the temperature instability ΔT is ±0.05 K, and the temperature uncertainty ΔT_c is lower than ±0.2 K. In order to reduce the blackbody temperature measurement uncertainty effect, relationship between blackbody irradiance and temperature are formed nonlinearly, which causes the temperature effect down to 0.1 K, and emissivity effects are alleviated through standard high-precision ground plane blackbody ($\varepsilon_m \geqslant 0.998$) placed in the vacuum.

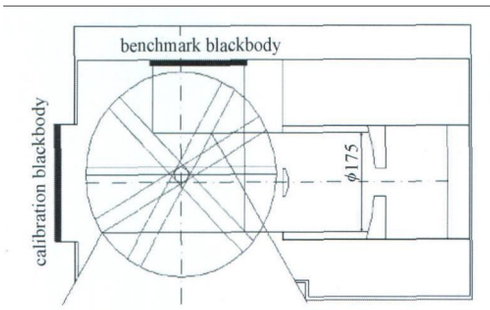

Fig. 1 On-board calibration two blackbodies arrangement

$$\begin{cases} L = (DN - b)/g \\ L = N_c/(\Delta\lambda \times \pi) \end{cases} \quad (1)$$

where L is radiance ($W \cdot m^{-2} \cdot \mu m^{-1} \cdot sr^{-1}$). DN is digital count. N_c is irradiance ($W \cdot m^{-2}$). $\Delta\lambda$ is the effective bandwidth (μm). b is the calibration bias (DN). g is the calibration gain ($DN \cdot W^{-1} \cdot m^2 \cdot sr \cdot \mu m$).

3 CALIBRATION AND RESULTS

3.1 DN calculation

HJ-1B IRS B08 arranges 10 detectors on sensor panel. Two hundred and twenty five times observations are carried out each on-board calibration process. The measurement values are mainly recorded in the blackbody state file (.rcp file) and sensor status file (.cal file). Cal documentation records the sensor response as digital count DN for 8 times, corresponding to the last eight columns in cal documents and calibration calculations take 8 DN mean values as effective value. Fig.2 is on-board calibration DN results on August 5, 2009 at normal and high temperature, respectively. Fig.3 is on-board calibration DN results on August 14, 2009 at normal and high temperature, respectively, in which DN_i stand for the digital count of the ith detector, and i is the detector sequence number.

3.2 Irradiance calculation

Rcp file contains calibration blackbody temperature T_c, and double-sided mirror left and right edge temperature T_{m_l} and T_{m_r}. Then according to former Eq.(2), we calculate N_{Tc} of the sensor in the optical system. Fig.4 shows the blackbody temperature T_c corresponding to different irradiance N_{Tc}.

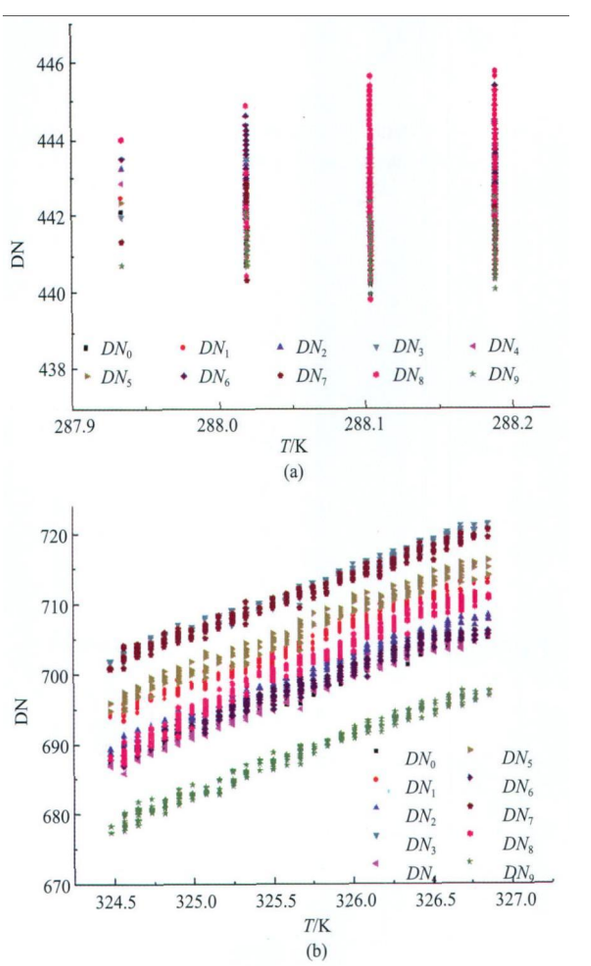

Fig. 2 On-board temperature VS DN on August 5, 2009
(a) Normal temperature; (b) High temperature

© 1994-2012 China Academic Journal Electronic Publishing House. All rights reserved. http://www.cnki.net

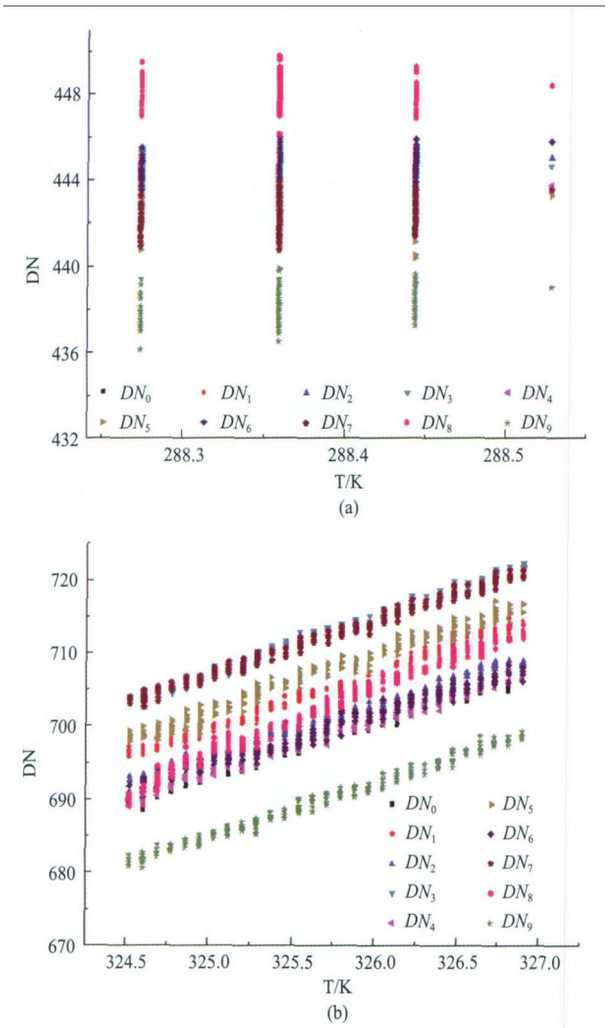

Fig. 3 On-board temperatures VS *DN* of August 14, 2009
(a) Normal temperature; (b) High temperature

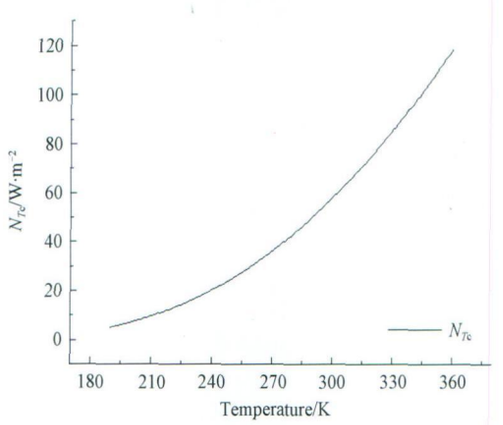

Fig. 4 Calibration blackbody temperature T_c VS irradiance N_{Tc}

$$N_{Tc} = k_0 + k_1 T_c + k_2 T_c^2 + k_3 T_c^3 \quad (2)$$

where N_{Tc} is irradiance(W·m^{-2}). k_i is a constant that measured in laboratory prelaunchly.

HJ-1B B08 imaging by double-sided mirror, and double-sided mirror contribute irradiance to the optical system, so correct the double-sided mirror irradiation contribution by Eq.(3) to get the corrected irradiance N_c, where a_{ci} and b_{ci} are double-sided mirror temperature correction constant. Fig.5 is on-board calibration N_c results on August 5, 2009 at normal and high temperature. Fig.6 is on-board calibration N_c results on August 14, 2009 at normal and high temperature.

$$\begin{cases} N_c = a_c + b_c \times N_{Tc} \\ a_c = a_{c0} + a_{c1} \times T_m \\ b_c = a_{c0} + b_{c1} \times T_m \\ T_m = (T_{m\_l} + T_{m\_r})/2 \end{cases} \quad (3)$$

3.3 Radiance translation

On-board calibration primary result irradiance N_c needs to be converted to radiance L through the effective bandwidth $\Delta\lambda$ by Eq.(1). $\Delta\lambda$ is the key point in the conversion process.

3.3.1 FWHM and MM methods

FWHM treats the effective bandwidth at half maximum response ($0.5R_{max}$), and it's experienced and simple, as shown in Fig. 7. MM calculates the effective bandwidth through effective wavelength, such as Eq.(4) shows (Palmer, 1984). Table 2 gives the two kinds of results calculated by FWHM and MM, and shows that FWHM and MM results are quite different at 20% relative difference.

$$\begin{cases} \Delta\lambda = 2\sqrt{3}\sigma \\ \sigma^2 = \int_{\lambda_{min}}^{\lambda_{max}} f(\lambda)\lambda^2 d\lambda \Big/ \int_{\lambda_{min}}^{\lambda_{max}} f(\lambda) d\lambda - \lambda_c^2 \\ \lambda_c = \int_{\lambda_{min}}^{\lambda_{max}} f(\lambda)\lambda d\lambda \Big/ \int_{\lambda_{min}}^{\lambda_{max}} f(\lambda) d\lambda \end{cases} \quad (4)$$

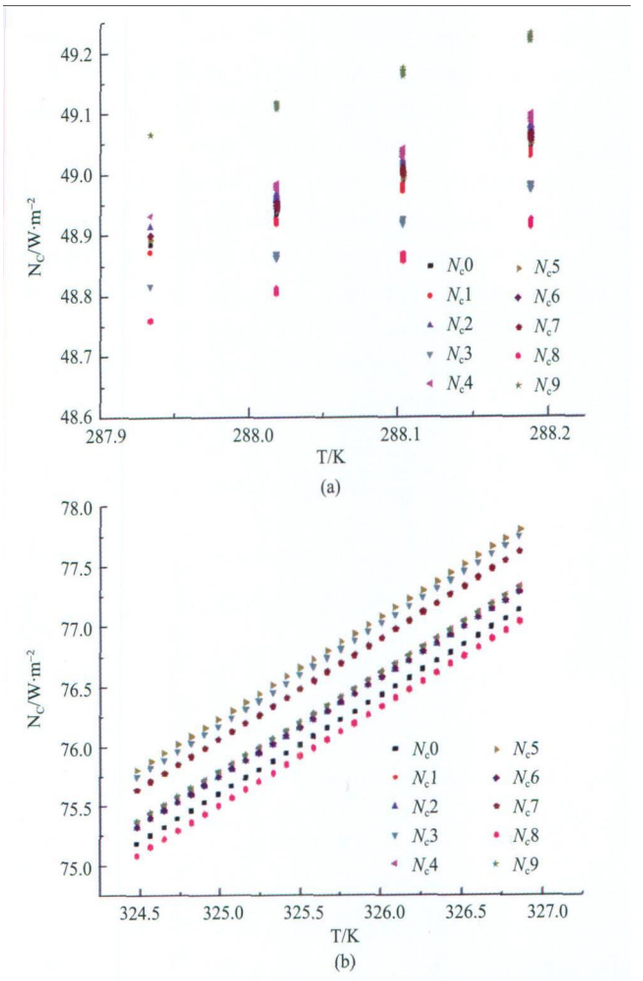

Fig. 5 On-board high temperature VS irradiance of August 5, 2009
(a) Normal temperature; (b) High temperature

© 1994-2012 China Academic Journal Electronic Publishing House. All rights reserved. http://www.cnki.net

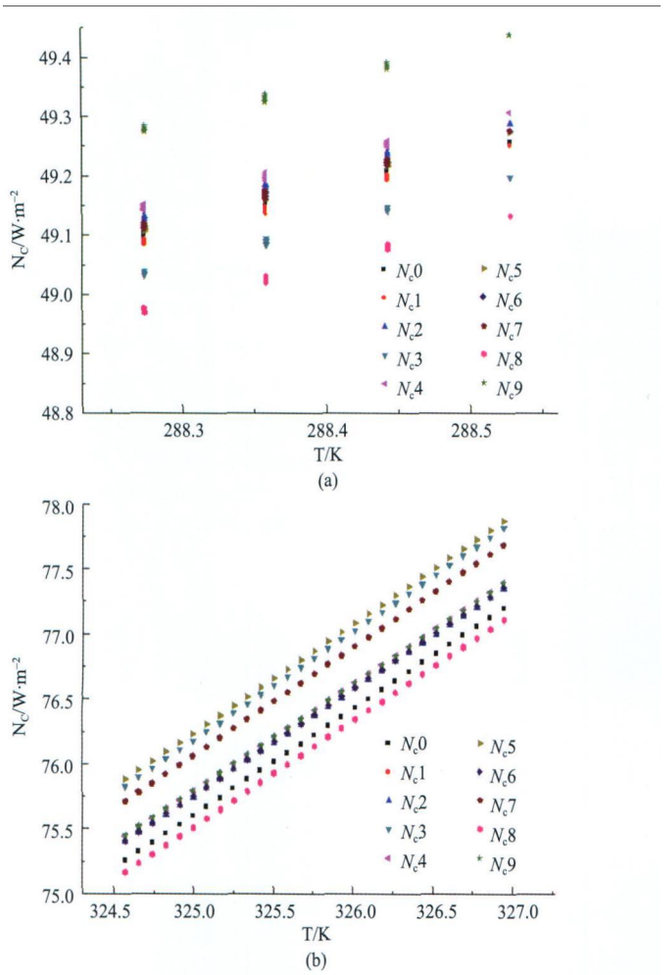

Fig. 6 On-board high temperature VS irradiance of August 14, 2009
(a) Normal temperature; (b) High temperature

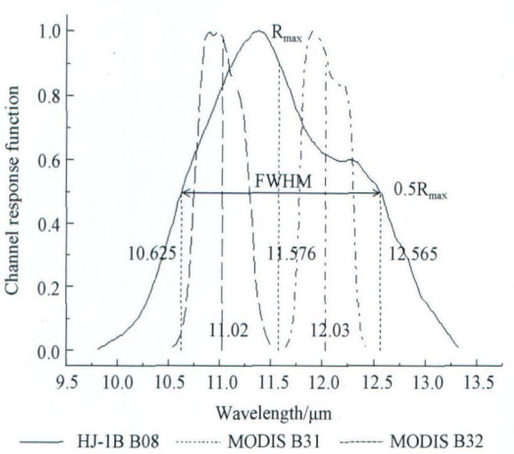

Fig. 7 FWHM method of effective bandwidth

Table 2 Effective bandwidth value of FWHM and MM methods

	FWHM/μm	MM/μm
Effective bandwidth	1.940	2.394

where $f(\lambda)$ is the sensor channel response function. λ_{max} and λ_{min} are the maximum and minimum wavelength boundary and the channel response function is zero outside this range.

3.3.2 LUT method

It's known from Eq.(1) that the effective bandwidth $\Delta\lambda$ is the function of irradiance and radiance, so it can be calculated if the blackbody irradiance and radiance by their ratio are known. Irradiance N_m of calibration blackbody is calculated by Eq.(2) through temperature T_m. Radiance L_m is calculated by the Planck function, channel response function(CRF) and blackbody emissivity ε_m, as the Eq.(5) shows (Rong, 2005; César, 2003). Then build $\Delta\lambda$ lookup table (LUT) by the ratio of N_m and πL_m at different blackbody temperatures T_m, calculated "look-up table method." When used in the process of on-board calibration, effective bandwidth is lookup by blackbody temperature. Effective bandwidth of the lookup table method results are shown in Fig.8 and Table 3, in which $\Delta\lambda$ linear varieties from 2.010 to 2.016 corresponding to 293±5 K normal temperature and 328±5 K high temperature, and the relative difference is 0.3% or less. Linear variation may be caused by temperature drift of calibration blackbody. $\Delta\lambda$ of lookup table method is between the results obtained by FWHM and MM. The impact of $\Delta\lambda$ effect on calibration results are specifically analysis below, and determine the optimal one.

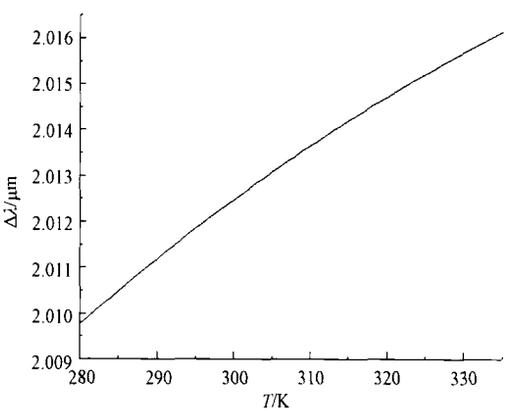

Fig. 8 Lookup table value of effective bandwidth

Table 3 Lookup table value of effective bandwidth

T/K	Δλ/μm	T/K	Δλ/μm
286	2.0106	312	2.0138
288	2.0109	314	2.0140
290	2.0111	316	2.0143
292	2.0114	318	2.0145
294	2.0117	320	2.0147
296	2.0119	322	2.0149
298	2.0122	324	2.0151
300	2.0124	326	2.0153
302	2.0127	328	2.0155
304	2.0129	330	2.0156
306	2.0131	332	2.0158
308	2.0134	334	2.0160
310	2.0136	336	2.0162

$$L_m = \frac{\int_{\lambda_{min}}^{\lambda_{max}} \varepsilon_m 2hc^2\lambda^{-5}(e^{\frac{hc}{\lambda kT_m}}-1)^{-1} f(\lambda)\mathrm{d}\lambda}{\int_{\lambda_{min}}^{\lambda_{max}} f(\lambda)\mathrm{d}\lambda} \quad (5)$$

where h is Planck constant, 6.626×10^{-34} J·s. k the Boltzmann constant, 1.3806×10^{-23} J·K^{-1}. c is the speed of light, 2.998×10^{8} m·s^{-1}.

© 1994-2012 China Academic Journal Electronic Publishing House. All rights reserved. http://www.cnki.net

3.4 Calibration results

It's known from Fig.2, Fig.3, Fig.5 and Fig.6 that HJ-1B B08 10 detectors themselves exist differences of DN and irradiance, which means detectors' response is not stable enough and a larger equivalent noise is existent. At the normal temperature, detectors' DN is different within 4 DN, and radiance is different within 0.02 $W \cdot m^{-2} \cdot \mu m^{-1} \cdot sr^{-1}$, which means the relative difference between the detectors is large. At the high temperature, detectors' DN is different within 2 DN, and radiance is different within 0.02 $W \cdot m^{-2} \cdot \mu m^{-1} \cdot sr^{-1}$, which means there are also relative differences. To reduce the count differences and radiance differences, average DN and radiance of all detectors are used in calibration process to obtain radiance L and DN at normal temperature and high temperature, and then obtain the calibration coefficients by linear regression under the different effective bandwidth as shown in Table 4.

Table 4 On-board calibration results

Date	(gain g/(DN·W^{-1}·m^2·sr·μm), bias b/DN)		
	FWHM	MM	LUT
2009-08-05	(57.457, −24.660)	(70.903, −24.661)	(59.920, −27.503)
2009-08-14	(56.995, −18.208)	(70.333, −18.208)	(59.438, −21.029)

4 RESULTS ANALYSE

Table 4 shows that calibration coefficients of FWHM, MM and LUT methods are different from each other. MM gets the largest gain and LUT method gets the largest bias. Using Terra-MODIS synchronized observation data and Qinghai Lake field experiment data to validate the calibration coefficients to analyze the applicability of the three bandwidths.

4.1 Analyzed based on MODIS

Calibrated HJ-1B IRS image over Qinghai Lake on August 12, 2009 04:22 (UTM) using three couples of coefficients of August 5 in Table 4 to get TOA radiance L, and then compared them with Terra-MODIS image B31,32 overpass at 04:18 (UTM) in the same day. The pixels in green lines is the amplified in red lines in Fig.13, which included sea-heart and experiment area, and Fig.15 are comparison of TOA radiance profile between MODIS B31,32 and HJ-1B B08, and Fig.14 is horizontal profile corresponding to horizontal line in Fig.13, and Fig.15 is vertical profile corresponding to vertical line in Fig.14. It can be known from Fig.14 and Fig.15 that TOA radiance of MM is lower than the other methods and TOA radiance of FWHM and LUT are located between MODIS B31 and B32, except that FWHM results are higher than that of MODIS on water surface.

Combination of Fig.11 about equivalent wavelength that HJ-1B B08' s is allocated between MODIS B31, 32's and thermal infrared radiactive transfer theory, MM gives a larger bandwidth than actual value and therefore the calibrated results are significantly lower, producing the maximum error.

4.2 Analyzed based on field measurement

Water body is an appropriate object used in validation for its temperature that not changed apparently in large area (Thome 1998; John, 2001; Barsi, 2003). Predicted TOA radiance of HJ-1B IRS B08 over Qinghai Lake in 12 August, 2009 using radiative transfer calculation based on the in situ measurements of atmosphere and water surface is shown as "experimental value" in Fig.9, Fig.10, Fig.11 and Fig.15, and Table 5 is the TOA radiance comparison between experimental value and vertical profile of water body. Tables and Figures show that FWHM gives a lower effective bandwidth that lead to a higher calibrated radiance and MM gives a lower calibrated radiance. LUT method result very approximate to experimental value and the difference of them is within 0.04 $W \cdot m^{-2} \cdot sr^{-1} \cdot \mu m^{-1}$.

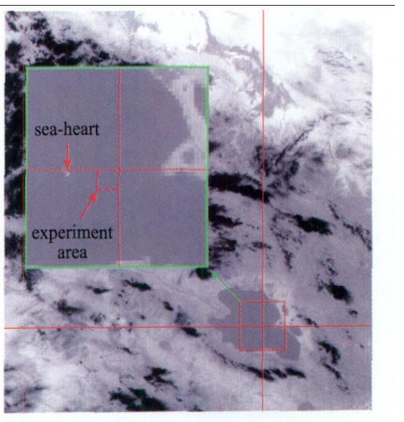

Fig. 9 HJ-1B B08 image of Qinghai lake area

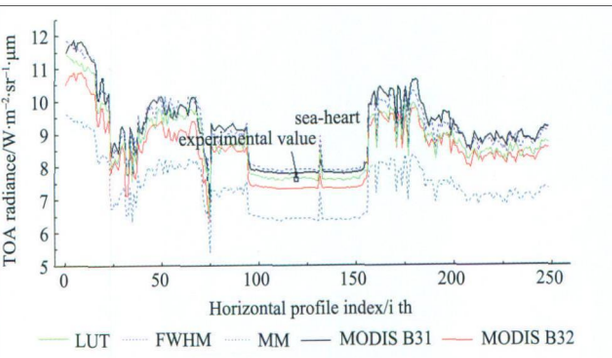

Fig. 10 Horizontal profiles of different calibration coefficient

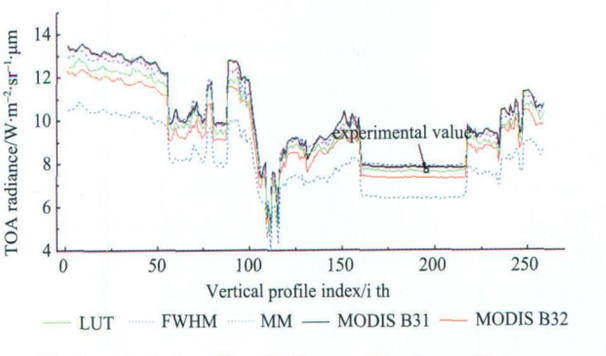

Fig. 11 Vertical profiles of different calibration coefficients

© 1994-2012 China Academic Journal Electronic Publishing House. All rights reserved. http://www.cnki.net

Table 5 Vertical profiles versus experiment value

Methods	TOA radiance $L/(W\cdot m^{-2}\cdot sr^{-1}\cdot \mu m^{-1})$	L difference $/(W\cdot m^{-2}\cdot sr^{-1}\cdot \mu m^{-1})$	L difference /%
Experimental value	7.61		
FWHM	7.93	0.32	4.20
MM	6.42	−0.81	−10.64
LUT	7.65	0.04	0.53

4.3 Two times comparison

As Table 4 shows there is a certain difference of bias b of the same method on August 5 and 14, but the gain g difference is not apparent. The difference of b is about 6 DN, since on-board calibration system is not stable enough at normal temperature with only changed in 1 K. The affection of b to radiance L is calculated by partial derivation of Eq.(1) showed as Eq.(7). The maximum difference of radiance L caused by b between these two times is 0.1 $W\cdot m^{-2}\cdot sr^{-1}\cdot \mu m^{-1}$, and the result on August 14 is the same as that on August 5.

$$e(\Delta b) = \partial L / \partial b \times \Delta b = -\Delta b / g \quad (6)$$

5 CONCLUSION

Effective bandwidth is one of the key parameters during the calculation of on-board calibration. LUT method, which was constructed by on-board calibration theory, pre-lunch experimental datum, channel relative reply, and Planck function composed a result that shifts from 2.010 μm to 2.016 μm corresponding to normal and high temperature. Effective bandwidth of LUT is distributed between that of FWHM and MM. The TOA radiance error of these three methods on Qinghai Lake surface are 0.32, −0.81, and 0.04 $W\cdot m^{-2}\cdot sr^{-1}\cdot \mu m^{-1}$, which lead to 3, −8, 0.4 K TOA temperature respectively. Instability of on-board calibration status at normal temperature of calibration blackbody lured 0.1 $W\cdot m^{-2}\cdot sr^{-1}\cdot \mu m^{-1}$ errors on TOA radiance, equally to 1 K TOA temperature error. For the character of HJ-1B IRS B08 channel response function, FWHM and MM are not suitable in the process of on-board calibration, and LUT can get a better on-board calibration result.

The ten detectors on HJ-1B IRS B08 are fluctuated with each other, so relative radiometric calibration need to be considered to get a higher accuracy of on-board calibration based on level zero images. Normal temperature status of calibration blackbody produces a direct affection on bias b, and an indirect affection on gain g. However, the affections on b and g are not independent for the change of bias b affect gain g, so it is necessary to substitute normal temperature status with ground-based measurement in filed experiment to enhance the accuracy of in-orbit radiometric calibration.

REFERENCES

Barsi J A, Schott J R, Palluconi F D, Helder D L, Hook S J, Markham B L, Chander G O'Donnell E M and Can. J. 2003. Landsat TM and ETM+ thermal band calibration. *Remote Sensing*, **29**(2): 141–153

César C, Vicente C, Enric V and Eva R. 2003. Validation of temperature-emissivity separation and split-window methods from TIMS data and ground measurements. *Remote Sensing of Environment*, **85**: 232–242

John R S, Barsi J A, Nordgren B L, Raqueño N G and Alwis D. 2001. Calibration of Landsat thermal data and application to water resource studies. *Remote Sensing of Environment*, **78**: 108–117

Lefevre M, Bauer O, Iehle A and Wald L. 2000. An automatic method for the calibration of time-series of Meteosat images. *Remote Sensing*, **21**(5): 1025–1045

Liang S L. 2009. Quantitative Remote Sensing. Beijing: Science press

Palmer J M. 1984. Effective bandwidths for Landsat-4 and Landsat-d' multispectral scanner and thematic maper subsystems. *IEEE Transactions on Geoscience and Remote Senssing*. **22**: 336–338

Rong Z G, Zhang Y X, Wang Y H, Qiu K M and Zhang R Y. 2005. Calibration method for water vapor channel of scanning-radiometer carried by FY-2B satellite. *Journal of Infrared and Millimeter Waves*. **24**(5): 357–365

Thome K, Arai K, Simon H, Kieffer H, Lang H, Matsunaga T, Ono A, Palluconi F, Sakuma H, Slater P, Takashima T, Tonooka H, Tsuchida S, Welch R M and Zalewski E. 1998. ASTER preflight and inflight calibration and the validation of level 2 products. *IEEE Transactions on Geoscience and Remote Sensing*. **36**(4): 1161–1171

Zhang Y. 2006. Study on Thermal Infrared Remote Sensor's Absolutely Radiometric Calibration. Beijing: Institute of Remote Sensing Applications, Chinese Academy of Sciences

© 1994-2012 China Academic Journal Electronic Publishing House. All rights reserved. http://www.cnki.net

HJ-1B B08在轨星上定标有效波段宽度计算的查找表法

李家国[1,2], 顾行发[1,2], 余涛[1,2], 韩启金[3], 郭宏[4], 王苏颖[5]

1. 中国科学院 遥感应用研究所, 北京 100101;
2. 中国科学院 研究生院, 北京 100049;
3. 中国资源卫星应用中心, 北京 100094;
4. 河南理工大学 测绘学院, 河南 焦作 454003;
5. 福建师范大学 地科学院, 福建 福州 350007

摘 要: 通过构建适用于HJ-1B热红外通道(IRSB08)特性的有效波段宽度计算方法, 提高HJ-1B B08在轨星上绝对辐射定标的精度。根据HJ-1B星上定标原理、利用卫星发射前地面实验数据和Planck方程, 建立基于定标黑体温度的有效波段宽度计算的查找表法, 结果表明查找表法得到的有效波段宽度为2.01 μm左右, 介于半高宽法1.940 μm和矩方法2.394 μm之间, 且与定标黑体温度的关联性很小, 在低温点和高温点之间的相对差异在0.3%以内。半高宽法和矩方法分别低估和高估有效波段宽度, 导致定标后的表观辐射亮度分别偏高和偏低, 不适用于HJ-1B B08特点, 查找表法定标的表观辐亮度与星地同步实验结果非常相近, 绝对误差为0.04 $W\cdot m^{-2}\cdot sr^{-1}\cdot \mu m^{-1}$, 对应的亮度温度误差为0.4 K左右, 能很好的应用于HJ-1B B08在轨星上绝对辐射定标。

关键词: HJ-1B, IRS, 定标, 有效波段宽度, 查找表法

中图分类号: TP732 **文献标志码:** A

引用格式: 李家国, 顾行发, 余涛, 韩启金, 郭宏, 王苏颖. 2011. HJ-1B B08在轨星上定标有效波段宽度计算的查找表法. 遥感学报, 15(1): 60–72

Li J G, Gu X F, Yu T, Han Q J, Guo H and Wang S Y. 2011. Lookup table method of effective bandwidth for HJ-1B B08 on-board radiometric calibration. *Journal of Remote Sensing*, 15(1): 60–72

1 引 言

HJ-1卫星是中国专门为环境保护和防灾减灾而发射的小卫星星座, 设计为2颗光学卫星和1颗雷达卫星的组合, 即"2+1"模式, 其中编号为B(简称HJ-1B)的光学卫星已于2008年9月发射升空。HJ-1B载荷为两台光学CCD传感器和一台红外成像仪IRS, 其中热红外波段(B08)参数设计如表1。精确的绝对辐射定标是遥感影像定量应用的前提条件(Lefevre等, 2000), 新一代卫星热红外传感器都具有星上定标系统, 如美国MODIS和TM传感器的全光路星上定标系统, 中国FY-2的半光路星上定标系统等(张勇, 2006)。HJ-1B采用的是全光路星上定标系统, 发射前HJ-1B热红外传感器测量的是黑体的辐照度N_c(单位: $W\cdot m^{-2}$), 而在定量遥感的实际应用过程中, 使用的是辐射亮度L(单位: $W\cdot m^{-2}\cdot \mu m^{-1}\cdot sr^{-1}$), N_c与L之间的相互转换需要考虑到传感器通道的有效波段宽度$\Delta\lambda$, $\Delta\lambda$的计算精度直接影响到定标精度。目前, $\Delta\lambda$的计算主要有峰值归一化法(peak method)、半高宽法(full width at half maximum)和Palmer(1984)提出的矩方法(moments method), 这些方法各有其特点和适用性。峰值归一化法以通道响应的最大值作为有效波长, 通过通道响应的积分面积除以有效波长求有效波宽, 误差较大, 不能估算波长界限; 半高宽法以通道响应峰值的一半($0.5R_{max}$)作为波长界限, 以波长上界和下界之间的距离来计算有效波宽, 中心波长即为有效波长; 矩方法融合了通道响应的特点, 以通道响应和波长的积分形式来求有效波宽,

收稿日期: 2010-03-15; **修订日期:** 2010-04-21

基金项目: 国家科技部中澳合作项目"中澳遥感定标与真值性检验联合研究计划"(编号: 2008DFA21540); 国防科技工业民用专项科研技术研究项目: HJ-1卫星数据应用研究(编号: 07K00100KJ)。

第一作者简介: 李家国(1982—), 男, 博士研究生, 主要从事红外遥感定标、火灾和地表温度定量反演研究。E-mail: jacoli@126.com。

© 1994-2012 China Academic Journal Electronic Publishing House. All rights reserved. http://www.cnki.net

有效波长和波长界限均有明确的计算公式(Liang, 2009)。本文针对 HJ-1B B08 通道响应函数(CRF)的特点, 以 2009 年 8 月 5 日和 14 日的星上定标数据为研究对象, 分析这些方法的适用性, 并对$\Delta\lambda$的计算方法进行改进, 构建适用于 HJ-1B B08 CRF 特点的$\Delta\lambda$计算方法, 提高在轨星上绝对辐射定标精度。

表 1 HJ-1B B08 设计参数

载荷	波段号	光谱范围/μm	空间分辨率/m	幅宽/km	重访周期/d
IRS	B08	10.5—12.5	300	720	4

2 HJ-1B 在轨星上定标原理

卫星发射前先通过在地面真空罐内的实验, 建立定标黑体温度与传感器接受到的辐照度之间的函数关系, 如式(2), 在轨星上定标期间, 通过观测外太空的冷空间来确定仪器背景辐射, 从而实现辐射基准, 即系统观测冷空间时的信号幅值在理论上为零电平, 但 HJ-1B IRS 传感器由于受到太阳帆板的遮挡作用无法观测冷空间, 因此利用星上两个黑体来实现星上定标, 其中基准黑体用来实现辐射基准, 校正黑体用来实现辐射校正, 系统观测基准黑体时探测器输出的信号值是相对于零辐射的一个绝对量, 两个黑体相对于光学系统扫描镜的位置如图 1。在轨绝对辐射定标期间, 探测器先采集校正黑体在常温点 293±5K 时的定标状态 $P_1(T_{c1}, DN_{c1})$, 再采集校正黑体被加热到高温点 328±5K 时的定标状态 $P_2(T_{c2}, DN_{c2})$, 通过地面实验建立的转换方程式(2)和式(3), 将 P_1 和 P_2 转换为 $P_1'(N_{c1}, DN_{c1})$和 $P_2'(N_{c2}, DN_{c2})$, 再代入式(1)进行回归得到在轨星上绝对辐射定标系数: 增益 g 和偏移 b。B08 波段基准黑体和校正黑体的比辐射率 $\varepsilon_c \geqslant 0.95$, 温度不稳定度 $\Delta T = \pm 0.05$ K, 温度被测量的不确定度 $\Delta T_c \leqslant \pm 0.2$ K。为了降低黑体温度测量不确定度带来的影响, 黑体温度和辐射量之间的非线性关系采用分段线性来等效, 从而将测温引起的非线性效应降低到 0.1K 以内, 比辐射率引起的误差通过置于真空罐内的高精度地面标准面源黑体($\varepsilon_m \geqslant 0.998$)来消除。

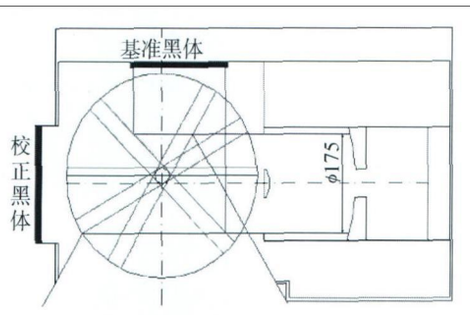

图 1 星上定标基准黑体和校正黑体相对位置

$$\begin{cases} L = (DN - b)/g \\ L = N_c/(\Delta\lambda \times \pi) \end{cases} \quad (1)$$

式中, L 为辐亮度, 单位: $W \cdot m^{-2} \cdot \mu m^{-1} \cdot sr^{-1}$, DN 为记数值。N_c 为辐照度, 单位: $W \cdot m^{-2}$, $\Delta\lambda$是有效波段宽度, 单位: μm。b 为定标偏移。g 为定标增益, 单位为: $DN \cdot W^{-1} \cdot m^2 \cdot sr \cdot \mu m$。

3 定标流程及结果

3.1 计数值计算

HJ-1B B08 波段共有 10 个扫描探元, 每次星上定标时共进行 225 帧测控, 测控参数主要记录在黑体状态文件(rcp 格式)和传感器状态文件(cal 格式)中。cal 文件记录了传感器对热辐射响应的计数值 DN, 定标时分别记录 8 次每帧每个探元的 DN 值, 对应于 cal 文件的最后 8 列, 定标计算时取 8 个 DN 值的均值作为传感器计数值的有效值。图 2(a)和(b)

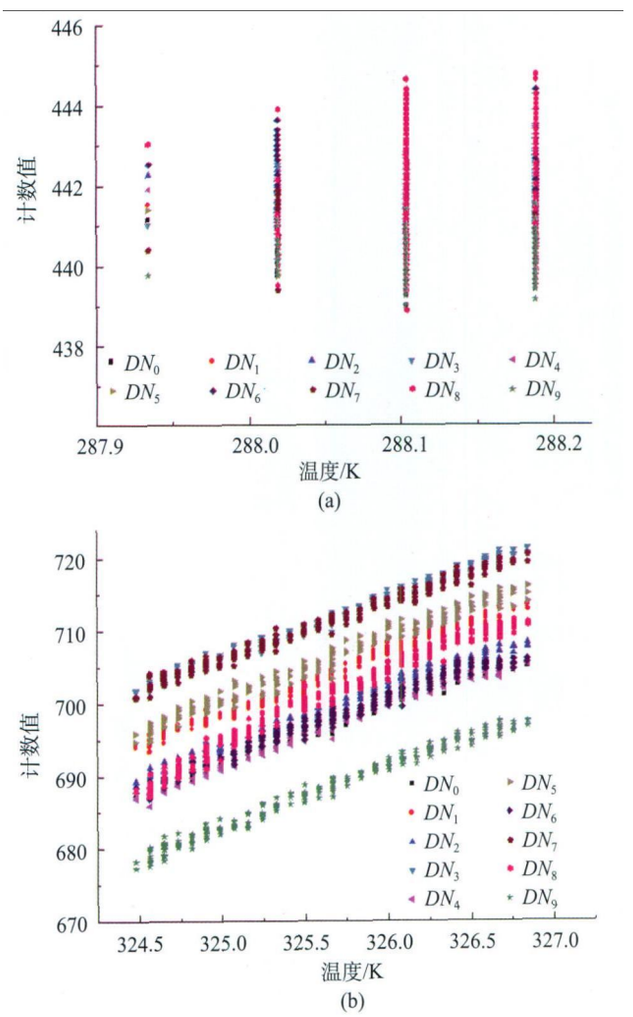

图 2 2009-08-05 星上定标常温计数值和高温点计数值
(a) 常温点计数值; (b) 高温点计数值

© 1994-2012 China Academic Journal Electronic Publishing House. All rights reserved. http://www.cnki.net

分为 2009-08-05 星上定标高温点和常温点计数值计算结果，图 3(a)和(b)分为 2009-08-14 星上定标高温点和常温点计数值计算结果。图中 DN_i 代表第 i 个扫描探元的计数值，i 为扫描探元的编号。

3.2 辐照度计算

rcp 文件包含了定标时校正黑体的温度 T_c 和双面镜左、右边缘温度 T_{m_l} 和 T_{m_r}，根据由地面标准面源黑体建立的式(2)计算校正黑体在温度 T_c 时传感器经由内部光路系统接收到的等效辐照度 N_{Tc}，图 4 为计算出来的不同黑体温度 T_c 对应的辐照度 N_{Tc} 曲线。

$$N_{Tc} = k_0 + k_1 T_c + k_2 T_c^2 + k_3 T_c^3 \tag{2}$$

式(2)中，N_{Tc} 单位 $W \cdot m^{-2}$，k_i 为发射前实验室测量的常数。B08 波段通过双面镜观测成像，双面镜温度对内部光路系统具有辐射贡献，因此通过式(3)对双面镜的辐射贡献进行纠正，得到纠正后的辐照度 N_c，式中 a_{ci} 和 b_{ci} 分别为双面镜温度纠正常数。图 5(a)和(b)分别为 2009-08-05 星上定标高温点和常温点辐照度计算结果，图 6(a)和(b)分别为 2009-08-14 星上定标高温点和常温点辐照度计算结果。

$$\begin{cases} N_c = a_c + b_c \times N_{Tc} \\ a_c = a_{c0} + a_{c1} \times T_m \\ b_c = a_{c0} + b_{c1} \times T_m \\ T_m = (T_{m\_l} + T_{m\_r})/2 \end{cases} \tag{3}$$

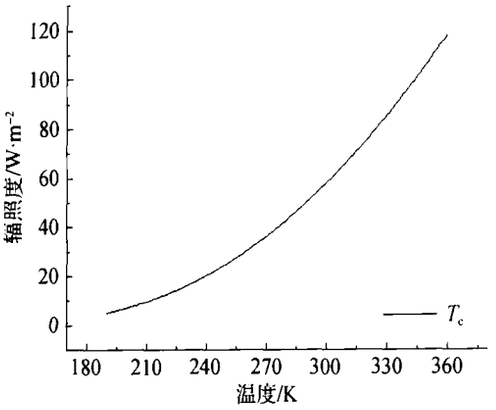

图 4 校正黑体温度 T_c 与等效辐照度 N_{Tc} 对应曲线

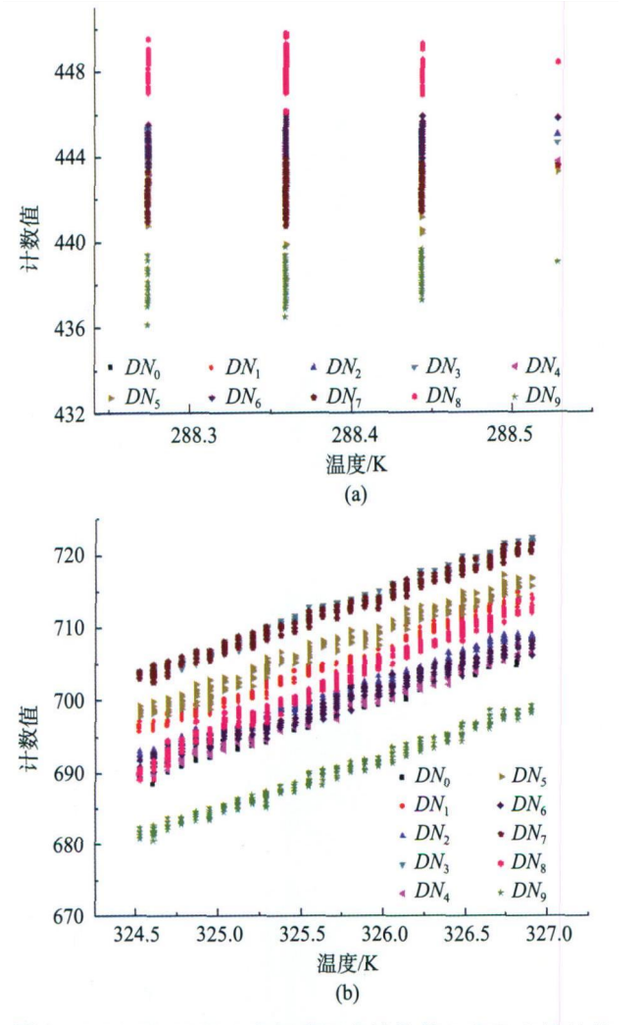

图 3 2009-08-14 星上定标常温点计数值和高温点计数值
(a) 常温点计数值; (b) 高温点计数值

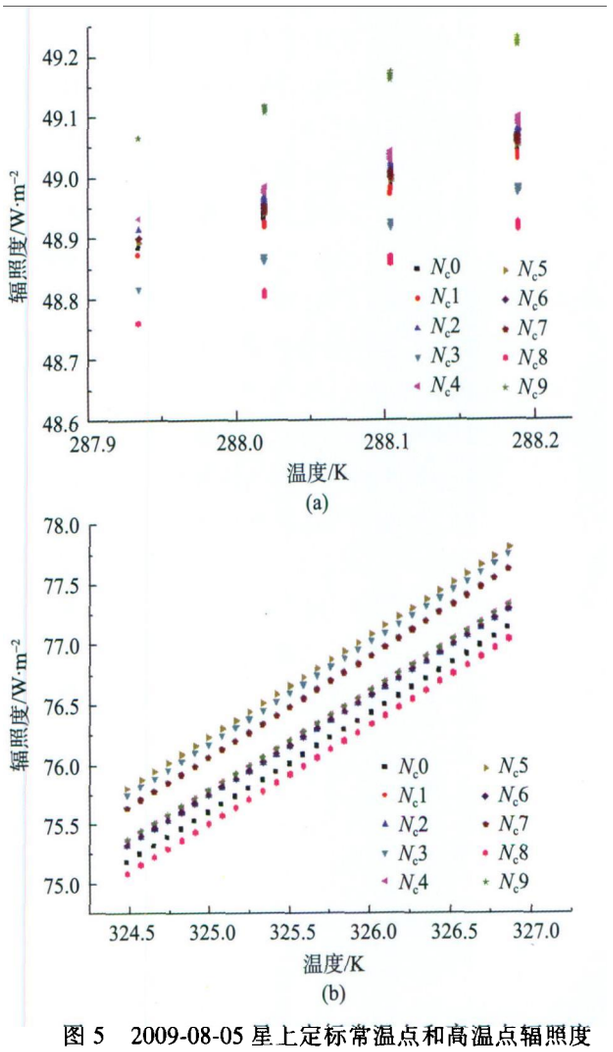

图 5 2009-08-05 星上定标常温点和高温点辐照度
(a) 高温点辐照度; (b) 常温点辐照度

© 1994-2012 China Academic Journal Electronic Publishing House. All rights reserved. http://www.cnki.net

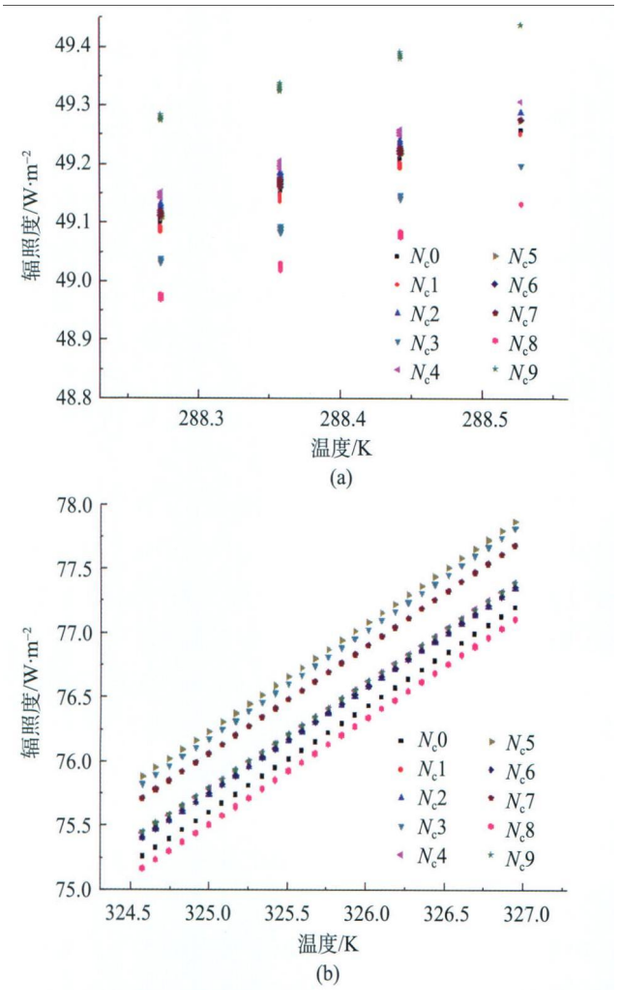

图 6 2009-08-14 星上定标常温点和高温点辐照度
(a) 常温点辐照度; (b) 高温点辐照度

3.3 辐亮度转换

星上定标系统获取的辐照度 N_c 需通过有效波段宽度 $\Delta\lambda$ 按式(1)转换为遥感应用中的辐亮度 L, 在转换过程中, 关键是精确计算有效波段宽度 $\Delta\lambda$。

3.3.1 半高宽法和矩方法

半高宽法以光谱最大响应的一半高度($0.5R_{max}$)来表示, 经验化且简单, 如图 7。矩方法通过中心波长来计算有效波段宽度, 如式(4)(Palmer, 1984)。表 2 为二种方法计算出的 $\Delta\lambda$ 结果, 从表中可知, 半高宽法和矩方法计算出的结果差异较大, 相对差异在 20%左右。

$$\begin{cases} \Delta\lambda = 2\sqrt{3}\sigma \\ \sigma^2 = \int_{\lambda_{min}}^{\lambda_{max}} f(\lambda)\lambda^2 \mathrm{d}\lambda \Big/ \int_{\lambda_{min}}^{\lambda_{max}} f(\lambda)\mathrm{d}\lambda - \lambda_c^2 \\ \lambda_c = \int_{\lambda_{min}}^{\lambda_{max}} f(\lambda)\lambda \mathrm{d}\lambda \Big/ \int_{\lambda_{min}}^{\lambda_{max}} f(\lambda)\mathrm{d}\lambda \end{cases} \quad (4)$$

式中, $f(\lambda)$ 为传感器通道响应函数, λ_{max} 和 λ_{min} 是波段响应的最大值和最小值, 在这个波段范围之外传感器的响应函数是零, 其他参数与前面相同。

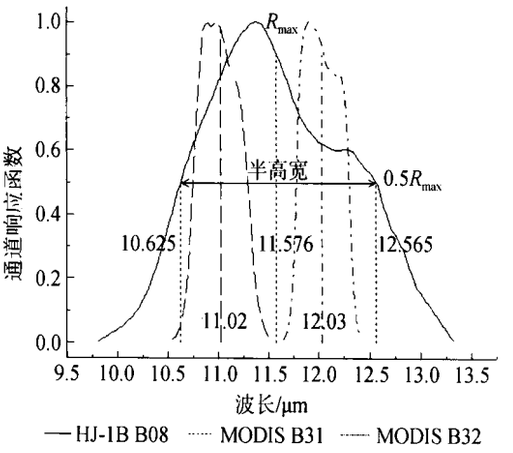

图 7 有效波段宽度计算的半高宽法

表 2 半高宽法和矩方法计算的有效波段宽度

	半高宽法/μm	矩方法/μm
有效波段宽度	1.940	2.394

3.3.2 查找表法

由式(1)可知, 有效波段宽度 $\Delta\lambda$ 是辐照度和辐亮度的函数, 因此可根据已知或求算的黑体辐照度和辐亮度的比值求出。黑体辐照度 N_m 利用式(2)由地面实验时的标准面源黑体温度 T_m 计算而来; 黑体辐亮度 L_m 由 Planck 公式卷积传感器通道响应函数(CRF)和比辐射率 ε_m 而来, 如式(5)所示(Rong, 2005; César 等, 2003)。通过 N_m 和 πL_m 的比值构建 $\Delta\lambda(T_m)$ 在不同黑体温度下的有效波段宽度查找表, 实现 $\Delta\lambda$ 计算的“查找表法”。在星上定标过程中再根据实际测量的黑体温度, 由查找表插值得到有效波段宽度。有效波段宽度查找法表计算结果如图 8 和表 3 所示, 从图 8 和表 3 可知, $\Delta\lambda$ 从星上定标常温点 293±5K 到高温点 328±5K, 由 2.010 近似线性变化到 2.016, 相对差异在 0.3%以内, 非常稳定。线性变化可能由星上定标的温度漂移造成。查找表法得到的 $\Delta\lambda$ 结果介于半高宽法和矩方法得到的结果之间, 不

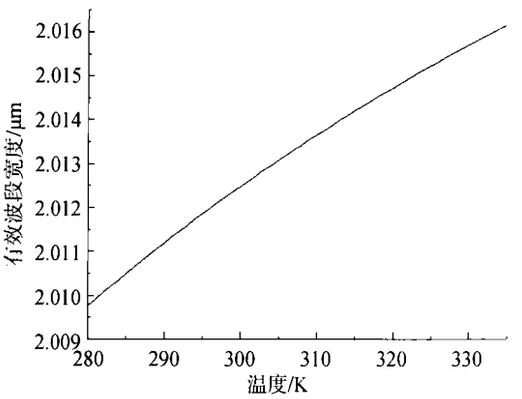

图 8 查找表法计算的有效波段宽度

© 1994-2012 China Academic Journal Electronic Publishing House. All rights reserved. http://www.cnki.net

表 3 查找表法计算的有效波段宽度

T/K	Δλ/μm	T/K	Δλ/μm
286	2.0106	312	2.0138
288	2.0109	314	2.0140
290	2.0111	316	2.0143
292	2.0114	318	2.0145
294	2.0117	320	2.0147
296	2.0119	322	2.0149
298	2.0122	324	2.0151
300	2.0124	326	2.0153
302	2.0127	328	2.0155
304	2.0129	330	2.0156
306	2.0131	332	2.0158
308	2.0134	334	2.0160
310	2.0136	336	2.0162

同方法得到的 $\Delta\lambda$ 对定标结果产生的影响在下文中深入分析，并确定最优值。

$$L_m = \frac{\int_{\lambda_{\min}}^{\lambda_{\max}} \varepsilon_m 2hc^2\lambda^{-5}(e^{\frac{hc}{\lambda kT_m}}-1)^{-1} f(\lambda)\mathrm{d}\lambda}{\int_{\lambda_{\min}}^{\lambda_{\max}} f(\lambda)\mathrm{d}\lambda} \quad (5)$$

式中，h 为 Planck 常数，取值 6.626×10^{-34}，单位：J·s，k 为玻耳兹曼常数，取值 1.3806×10^{-23}，单位：$J\cdot K^{-1}$，c 为光速，取值 2.998×10^{8}，单位：$m\cdot s^{-1}$，其他参数与前面相同。

3.4 定标结果

由图 2—图 3 的计数值和图 5—图 6 的辐照度值可知，HJ-1B B08 传感器的 10 个探元本身及相互之间存在着相对计数差异和辐照度差异，探元响应状态不够稳定，即通道等效噪声较大。在常温点时，探元本身的计数差异在 4 DN 左右，辐亮度差异在 0.02 $W\cdot m^{-2}\cdot\mu m^{-1}\cdot sr^{-1}$ 左右，探元之间的相对差异较大；在高温点时，探元本身的计数差异在 2DN 左右，辐亮度差异在 0.02 $W\cdot m^{-2}\cdot\mu m^{-1}\cdot sr^{-1}$ 左右，线性变化较为稳定，探元之间也存在一定的相对差异。为了降低计数差异和辐亮度差异的影响，对所有探元的响应作均值处理，分别得到常温点和高温点的辐亮度 L 及计数值 DN，再通过线性回归，得到在不同有效波段宽度下的定标系数(见表 4)。

表 4 2009-08-05 和 2009-08-14 星上绝对辐射定标结果

时间	增益 g/(DN·W⁻¹·m²·sr·μm)，偏移 b		
	半高宽法	矩方法	查找表法
2009-08-05	(57.457, −24.660)	(70.903, −24.661)	(59.920, −27.503)
2009-08-14	(56.995, −18.208)	(70.333, −18.208)	(59.438, −21.029)

4 结果比对与分析

由表 4 可知，半高宽法、矩方法和查找表法得到的定标系数相互之间存在差异，矩方法增益最大，半高宽法与查找表法相近，查找表法偏移最大，半高宽法和矩方法相近。以 Terra-MODIS 数据和星地同步观测实验数据比对不同定标系数得到的 HJ-1B B08 表观辐亮度，进而分析不同有效波段宽度计算方法的精度及适用性。

4.1 基于 MODIS 数据分析

利用表 4 中 2009-08-05 三组星上定标结果，分别定标 2009-08-12 04 点 22 分(UTM)过境于中国定标与真实性检验场地之一的青海湖湖区遥感影像(图 9)，得到不同定标系数下的表观辐亮度 L，并与同天 04 点 18 分(UTM)过境的 Terra-MODIS 传感器第 31 波段和 32 波段数据进行比较。图 9 中绿色边框内的数据为红色矩形框内的数据的放大视图，包含海心山和实验区。

图 10 和图 11 分别为 MODIS B31,B32 和 HJ-1B B08 表观辐亮度的剖面比对。图 10 为图 9 中贯穿整幅影像区域的水平红色线条所在位置的水平方向剖面，图 10 为图 9 中贯穿整幅影像区域的垂直红色线条所在位置的垂直方向剖面。由图 10 和图 11 可知，矩方法值低于所有其他值，半高宽法值和查找表法值基本介于 MODIS B31,B32 之间，但半高宽法在水体地物处明显高于 MODIS 值。结合图 7 中 HJ-1B B08 等效中心波长位于 MODIS B31，B32 中间及热红外辐射传输理论可知，矩方法过高计算了通道有效波段宽度，定标结果明显偏低，误差最大。

4.2 基于星地同步观测数据分析

由于水体在大范围内温度变化不大且近似于黑

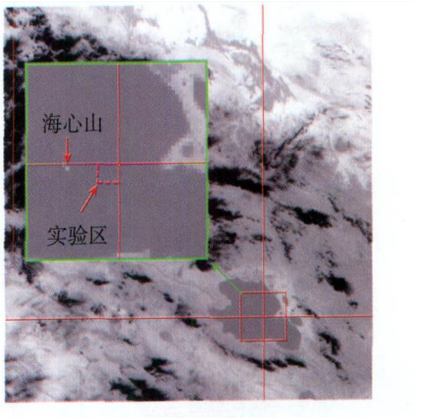

图 9 青海湖湖区 HJ-1B B08 遥感影像

© 1994-2012 China Academic Journal Electronic Publishing House. All rights reserved. http://www.cnki.net

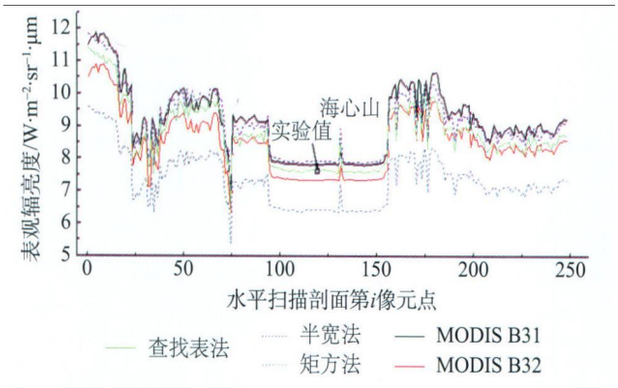

图 10 不同定标系数得到的水平剖面辐亮度

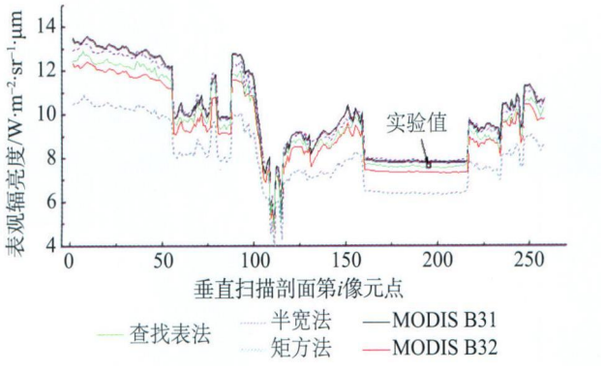

图 11 不同定标系数得到的垂直剖面辐亮度

体，因此是定标与真实性检验的倾向性目标之一(Thome 等, 1998; John 等, 2001; Barsi 等, 2003)。基于 2009 年 8 月 12 日卫星过境时刻在青海湖实验区(如图 9 所示)获取的星地同步观测水表参数和大气探空廓线，利用热红外辐射传输方程计算 HJ-1B B08 在卫星入瞳处的表观辐亮度，结果如图 10 和图 11 中“实验值”所示。表 5 为实验值与水体垂直剖面表观辐亮度均值的比对。结合图表可知，半高宽法过低计算了通道有效波段宽度，定标结果偏高，矩方法定标结果偏低，查找表法结果与实验值非常接近，表观辐亮度绝对误差为 0.04 $W\cdot m^{-2}\cdot sr^{-1}\cdot\mu m^{-1}$。

表 5 水体垂直剖面表观辐亮度均值与实验值比对

方法	表观辐亮度 L /$W\cdot m^{-2}\cdot sr^{-1}\cdot\mu m^{-1}$	L 差异 /$W\cdot m^{-2}\cdot sr^{-1}\cdot\mu m^{-1}$	L 差异 /%
实验值	7.61		
半高宽法	7.93	0.32	4.20
矩方法	6.42	−0.81	−10.64
查找表法	7.65	0.04	0.53

4.3 不同时间结果分析

由表 4 可知, 2009-08-14 和 2009-08-05 同一计算方法得到的增益 g 相近，但偏移 b 有一定的差异，偏移 b 的差异均为 6 个 DN 左右，产生的主要原因是由于星上定标系统在常温点时不够稳定，且常温点只在温度变化 1K 以内测控，温差序列不足。结合偏移 b 的实际差异，通过计算式(1)的偏导分析偏移 b 的变化对定标结果 L 的影响，结果如式(6)。将两次定标结果代入式(6)可知，两次偏移 b 的差异对表观辐亮度 L 最大会产生 $0.1W\cdot m^{-2}\cdot sr^{-1}\cdot\mu m^{-1}$ 的差异。应用 2009-08-14 定标系数产生的结论与 2009-08-05 一致。

$$e(\Delta b)=\partial L/\partial b\times\Delta b=-\Delta b/g \tag{6}$$

5 结 论

通道有效波段宽度是星上定标实施过程中的重要参数，基于 HJ-1B 星上定标原理，利用发射前地面实验数据和 Planck 方程，构建有效波段宽度计算的查找表法，结果显示查找表法计算的有效波段宽度从常温点的 2.010 μm 变化到高温点的 2.016 μm，非常稳定，介于半高宽法和矩方法得到的有效波段宽度之间。通过比对分析不同定标系数计算出的 HJ-1B B08、MODIS B31,B32 及星地同步观测实验的表观辐亮度可知，半高宽法、矩方法和查找表法生成的表观辐亮度绝对误差分别为 0.32、−0.81 和 0.04 $W\cdot m^{-2}\cdot sr^{-1}\cdot\mu m^{-1}$，对应的亮温差异分别在 3 K、−8 K 和 0.4 K 左右。由星上常温点温差较小、温度序列不足而引起的偏移 b 的不稳定性对表观辐亮度 L 会产生 0.1 $W\cdot m^{-2}\cdot sr^{-1}\cdot\mu m^{-1}$ 的差异，对应的亮温差异在 1 K 左右。由于 HJ-1B B08 通道响应的特性，半高宽法和矩方法并不适用于 HJ-1B B08 通道有效波段宽度的计算，基于发射前地面实验数据构建的查找表法，能很好的应用于星上定标。

HJ-1B B08 不同探元之间存在相对差异，因此高精度的星上定标需要基于零级数据对探元之间的相对差异进行纠正。星上常温点的状态对偏移 b 的稳定性存在较大的直接影响，对增益 g 存在间接影响，对两者的影响并不相互独立，因为偏移 b 的改变会间接改变增益 g，因此有必要以地面星地同步观测数据替代星上常温点数据，从而提高 HJ-1B B08 在轨绝对辐射定标精度。

REFERENCES

Barsi J A, Schott J R, Palluconi F D, Helder D L, Hook S J, Markham B L, Chander G O'Donnell E M and Can. J. 2003. Landsat TM and ETM+ thermal band calibration. *Remote*

© 1994-2012 China Academic Journal Electronic Publishing House. All rights reserved. http://www.cnki.net

Sensing, **29**(2): 141–153

César C, Vicente C, Enric V and Eva R. 2003. Validation of temperature-emissivity separation and split-window methods from TIMS data and ground measurements. *Remote Sensing of Environment*, **85**: 232–242

John R S, Barsi J A, Nordgren B L, Raqueño N G and Alwis D. 2001. Calibration of Landsat thermal data and application to water resource studies. *Remote Sensing of Environment*, **78**: 108–117

Lefevre M, Bauer O, Iehle A and Wald L. 2000. An automatic method for the calibration of time-series of Meteosat images. *Remote Sensing*, **21**(5): 1025–1045

Liang S L. 2009. Quantitative Remote Sensing. Beijing: Science press

Palmer J M. 1984. Effective bandwidths for Landsat-4 and Landsat-d' multispectral scanner and thematic maper subsystems. *IEEE Transactions on Geoscience and Remote Senssing*. **22**: 336–338

Rong Z G, Zhang Y X, Wang Y H, Qiu K M and Zhang R Y. 2005. Calibration method for water vapor channel of scanning-radiometer carried by FY-2B satellite. *Journal of Infrared and Millimeter Waves*. **24**(5): 357–365

Thome K, Arai K, Simon H, Kieffer H, Lang H, Matsunaga T, Ono A, Palluconi F, Sakuma H, Slater P, Takashima T, Tonooka H, Tsuchida S, Welch R M and Zalewski E. 1998. ASTER preflight and inflight calibration and the validation of level 2 products. *IEEE Transactions on Geoscience and Remote Sensing*. **36**(4): 1161–1171

Zhang Y. 2006. Study on Thermal Infrared Remote Sensor's Absolutely Radiometric Calibration. Beijing: Institute of Remote Sensing Applications, Chinese Academy of Sciences

附中文参考文献

梁顺林. 2009. 定量遥感. 北京: 科学出版社

戎志国, 张玉香, 王玉花, 邱康睦, 张如意. 2005. 风云二号B星星载扫描辐射计水汽通道定标方法. 红外与毫米波学报, **24**(5): 357–365

张勇. 2006. 遥感传感器热红外数据辐射定标研究. 北京: 中国科学院研究生院

© 1994-2012 China Academic Journal Electronic Publishing House. All rights reserved. http://www.cnki.net